

Organic Semiconducting Nanoparticles as Efficient Photoacoustic Agents for Lightening Early Thrombus and Monitoring Thrombolysis in Living Mice

Cao Cui,^{†,§} Zhen Yang,^{‡,§} Xiang Hu,[†] Jinjun Wu,[‡] Kangquan Shou,[†] Hengheng Ma,[‡] Chao Jian,[†] Yong Zhao,[†] Baiwen Qi,[†] Xiaoming Hu,[‡] Aixi Yu,^{*,†} and Quli Fan^{*,‡,§}

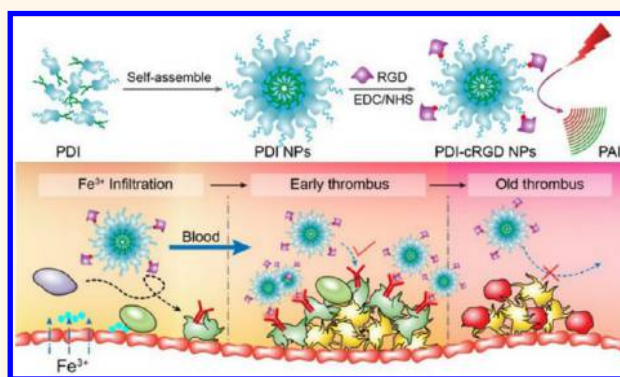
[†]Department of Orthopedics, Zhongnan Hospital of Wuhan University, Wuhan, Hubei 430071, China

[‡]Key Laboratory for Organic Electronics and Information Displays & Institute of Advanced Materials (IAM), Jiangsu National Synergetic Innovation Center for Advanced Materials (SICAM), Nanjing University of Posts & Telecommunications, Nanjing 210023, China

Supporting Information

ABSTRACT: Acute venous thrombosis is prevalent and potentially fatal. Accurate diagnosis of early thrombus is needed for patients in timely clinical intervention to prevent life-threatening conditions. Photoacoustic imaging (PAI) with excellent spatial resolution and high optical contrast shows more promise for this purpose. However, its application is dramatically limited by its signal-off effect on thrombus because of the ischemia in thrombus which lacks the endogenous photoacoustic (PA) signal of hemoglobin. To address this dilemma, we herein report the feasibility of using organic semiconducting nanoparticles (NPs) for contrast-enhanced PAI of thrombus in living mice. An organic semiconducting NP, self-assembled by amphiphilic perylene-3,4,9,10-tetracarboxylic diimide (PDI) molecules, is chemically modified with cyclic Arg-Gly-Asp (cRGD) peptides as a PA contrast agent (cRGD-PDI NPs) for selectively lightening early thrombus. cRGD-PDI NPs presents high PA intensity, good stability in light and serum, and sufficient blood-circulating half-life. In living mice, PA intensity of early thrombus significantly increases after tail vein injection of cRGD-PDI NPs, which is 4-fold greater than that of the control, blocking, and old thrombus groups. Pathological and immunohistochemical findings show that glycoprotein IIb/IIIa abundant in early thrombus is a good biomarker targeted by cRGD-PDI NPs for distinguishing early thrombus from old thrombus by PAI. Such a lightening PAI effect by cRGD-PDI NPs successfully provides accurate information including the profile, size and conformation, and spatial distribution of early thrombus, which may timely monitor the obstructive degree of thrombus in blood vessels and the thrombolysis effect.

KEYWORDS: PDI nanoparticles, photoacoustic imaging, contrast agent, early thrombus, NIR absorption



Venous thromboembolism (VTE), including deep-vein thrombosis (DVT) and pulmonary embolism (PE), has a high incidence of disease around the world and can be potentially life-threatening.¹ The estimated incidence rate of DVT in industrialized countries is 1–3% per year.² Among these DVT patients, up to 50% will develop into more serious post-thrombotic syndrome (PTS), including pain, cramping, swelling, and heaviness.³ What's more, the recurrent DVT occurring up to 10% per year in unprovoked DVT patients further increases the risk of PTS, PE, and death.⁴ Currently, the treatment toward thrombus mainly includes two types. Early thrombus can be removed by thrombolytic drugs to recanalize

the vein, whereas old thrombus can only be treated with anticoagulants to prevent thrombus expansion.⁵ Thereby, rapid yet accurate diagnosis of early thrombus for timely clinical intervention as well as potential prevention of further life-threatening complications is of tremendous importance.⁶ The existing technique for thrombus detection includes computed tomography (CT), magnetic resonance imaging (MRI),

Received: January 26, 2017

Accepted: February 27, 2017

Published: February 27, 2017

positron emission tomography (PET), and ultrasound (US). However, the ionizing radiation-based CT⁶ and PET⁷ suffer radiation risks. MRI can provide detailed anatomic reference information but shares the drawbacks of weak functional signals, suboptimal spatial resolution, and time-consuming examination processes.^{8,9} In addition to the expensive costs of PET and MRI examination, those bulky instruments for PET and MRI are unmovable and consequently inconvenient for some special patients who cannot walk or are in critical conditions. Clinically, US has become the primary imaging tool for VET diagnosis because of its widespread availability, real-time image, high penetration depth, portability, and safety.¹⁰ However, the difficulty of the US technique to discern abnormalities from surrounding tissue greatly limits its further application owing to the similar acoustic impedances. Consequently, exploring appropriate imaging techniques to provide more accurate information on early thrombus is highly desired.

Photoacoustic imaging (PAI) is a non-ionizing and hybrid imaging paradigm that integrates optical excitation and ultrasonic detection. Thus, it provides an attractive feature of excellent spatial resolution and high optical contrast for data collection.¹¹ Given these merits, PAI has been developed rapidly for preclinical studies on vascular biology, oncology, neurology, cardiology, dermatology, ophthalmology, and gastroenterology. Although the clinical application of PAI is still limited by light penetration depth (1–5 cm) at present,¹² some pioneering studies in clinical research for humans have been forging ahead.^{13,14} Because of the extremely enhanced light absorption of hemoglobin relative to surrounding tissues, the light-absorption-based PAI technique exhibits tremendous advantages in visually distinguishing the blood vessels from surrounding tissues. It is well-known that thrombosis will cause the alterations to the erythrocyte and finally influence the number and quality of hemoglobin. Therefore, this is theoretically applicable to detect thrombus by PAI on the basis of the difference of hemoglobin.¹⁵ Indeed, present PAI on venous thrombus showed reduced intensity (signal-off) because of ischemia, which lacks an endogenous chromophore (e.g., oxyhemoglobin).^{15,16} Unfortunately, in this way, it is really difficult to differentiate the photoacoustic (PA) signals between the thrombus and the background, let alone the accurate location, size, shape, and other information on the thrombus to further distinguish early thrombus from old thrombus. Therefore, it is of paramount importance to specifically lighten early thrombus by employing a PA contrast agent. When the position of intravascular thrombus staying in the blood vessel is taken into account, the prerequisite features of a good PA contrast agent should include various improved properties, such as sufficient circulating time, stability in light and blood, high target selectivity, high light absorption intensity, low toxicity, and good water solubility.^{17–19} However, as far as we know, no efficient PA contrast agent for the detection of early thrombus has been reported.

Recently, various near-infrared (NIR) light (having deeper penetration for *in vivo* imaging compared to visible light) absorptive materials, such as metallic nanomaterials (e.g., gold nanorods,²⁰ gold nanovesicles²¹), up-conversion nanoparticles (NPs),²² carbonaceous nanomaterials (e.g., graphene,²³ carbon nanotubes,²⁴ and polyhydroxyfullerenes²⁵), organic dyes,²⁶ and organic semiconducting NPs^{27–30} have been developed as contrast agents to enhance PA signals in imaging of angiogenesis, tumor microenvironments, microcirculation,

biomarkers, brain functions, drug response, and gene activities. In such, organic materials receive increasing attention mainly due to their relatively good biocompatibility and easy chemical modification to provide their various photophysical properties, water solubility, biocompatibility, and targeting ability. For example, indocyanine green and methylene blue, the Food and Drug Administration (FDA) approved NIR dyes, have been widely used for PAI study despite their poor light stability.³¹ However, their NIR absorption (extinction coefficient, $\epsilon = 10^4$ to $10^5 \text{ M}^{-1} \text{ cm}^{-1}$) is insufficient to generate an obvious PA signal.^{31,32} In comparison, organic NPs having molecular aggregation exhibit a much higher absorption property ($\epsilon = 10^8$ to $10^9 \text{ M}^{-1} \text{ cm}^{-1}$) and better photostability than the monomer, which have been widely adopted for *in vivo* PAI.³¹ In consideration of the hydrophobicity of most PA signal-generated molecules, they are generally blended with amphiphilic molecules to form NPs to realize their water solubility and biocompatibility.³³ The blending method is further applied to combine different PA contrast agents together to simply realize ratiometric PA probes.^{27,34} Unfortunately, those encapsulated organic dyes by the blending method was observed to be leaching out more or less from the NPs *in vivo*, which may cause unexpected pseudosignals.^{17,35}

Herein, we rationally designed cyclic Arg-Gly-Asp (cRGD) peptide-modified NIR-absorptive organic semiconducting NPs self-assembled by amphiphilic perylene-3,4,9,10-tetracarboxylic diimide (PDI) derivatives and successfully realized it as an efficient PA contrast agent for selectively lightening early thrombus in living mice. The design of the molecular structure is based on these considerations: (1) Organic semiconducting molecules as PA contrast agents generally exhibit good light absorption and photostability.²⁷ As a typical organic semiconducting molecule, PDI has received great attention in bioelectronics and biomedical applications due to its high chemical, thermal, and photochemical stabilities as well as outstanding optoelectronic property and easy modification.^{36,37} In our previous works, we successfully employed a NIR-absorptive PDI derivative for PAI of a deep brain tumor in living mice.³⁸ (2) A hydrophobic alkyl chain and a hydrophilic polyethylene glycol (PEG) chain were covalently bonded to the PDI group to form an amphiphilic structure for self-assembling into NPs in water. The combination of the strong π - π interaction among planar PDI molecules,³⁸ the van der Waals' force of the alkyl chain, and the hydrophobic and hydrophilic interactions in one entity constructed by a single component contributes to enhance the NPs' stability in blood. Also, the hydrophilic PEGs lying on the NP's surface provide NPs with a long circulating time and good biocompatibility *in vivo*.³⁹ Furthermore, the formed PDI aggregation in the NPs is good for strengthening PA signals. (3) Platelet activation is a common pathophysiological process that occurs in the early stages of thrombus. Thus, imaging of activated platelets promises the sensitive detection of early thrombus.^{40,41} Glycoprotein IIb/IIIa (GPIIb/IIIa), a heterodimeric glycoprotein as a bridge between activated platelets, is essential in the development of platelet aggregation and thrombosis. It undergoes conformational changes from a low-affinity to a high-affinity state when platelets are activated in early thrombus and then from a high-affinity to a low-affinity state when early thrombus grows into old thrombus.^{42,43} These features make GPIIb/IIIa a suitable biomarker of early thrombus. cRGD peptide has been proven to have a high binding affinity to GPIIb/IIIa when platelet-activated in the early stage of

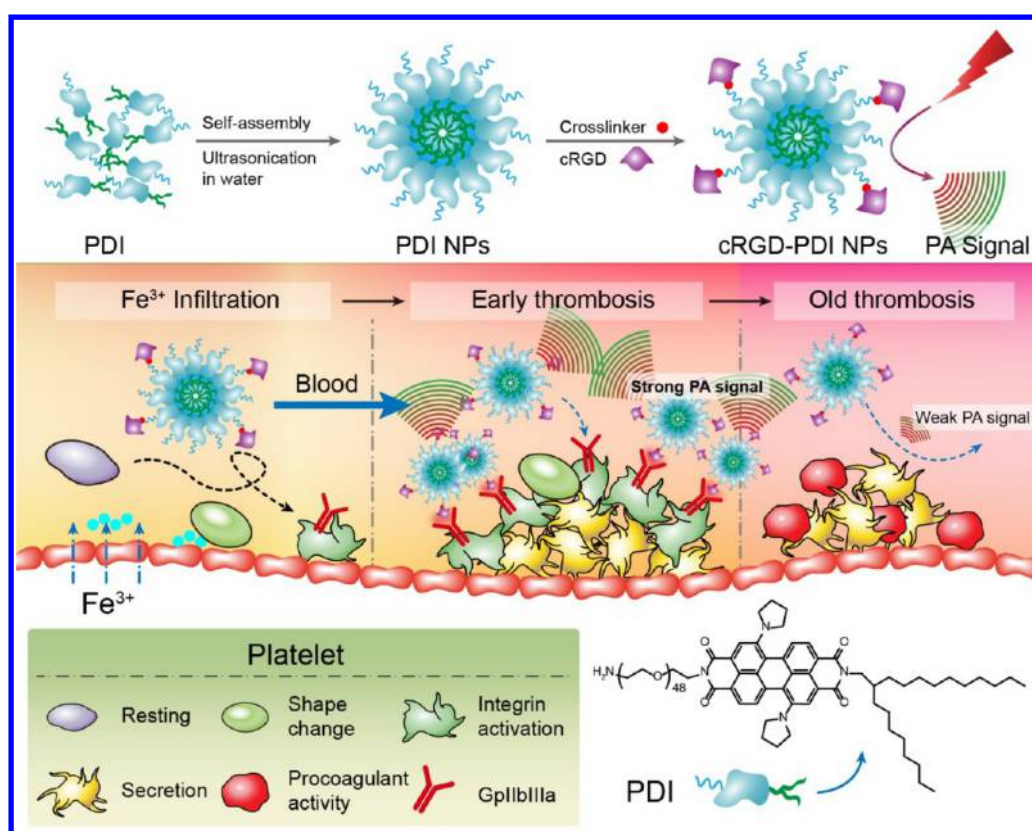


Figure 1. Schematic illustration of the preparation of cRGD-PDI NPs and its mechanism for specifically lightening early thrombus by PAI. For PAI, 5% FeCl_3 was applied to the jugular vein and diffused through the vessel wall, resulting in the exposure of basement membrane components to circulating blood cells. Platelets were then activated to deform, adhere, and aggregate together to form early thrombus during the vascular intima injury. The initial resting integrin GPIIb/IIIa on the platelets transformed into a high-affinity state in early thrombus and finally became a low-affinity state when the early thrombus grew into an old thrombus. cRGD-PDI NPs can target GPIIb/IIIa in early thrombus while inefficiently in old thrombus, resulting in selectively lightening early thrombus by PAI.

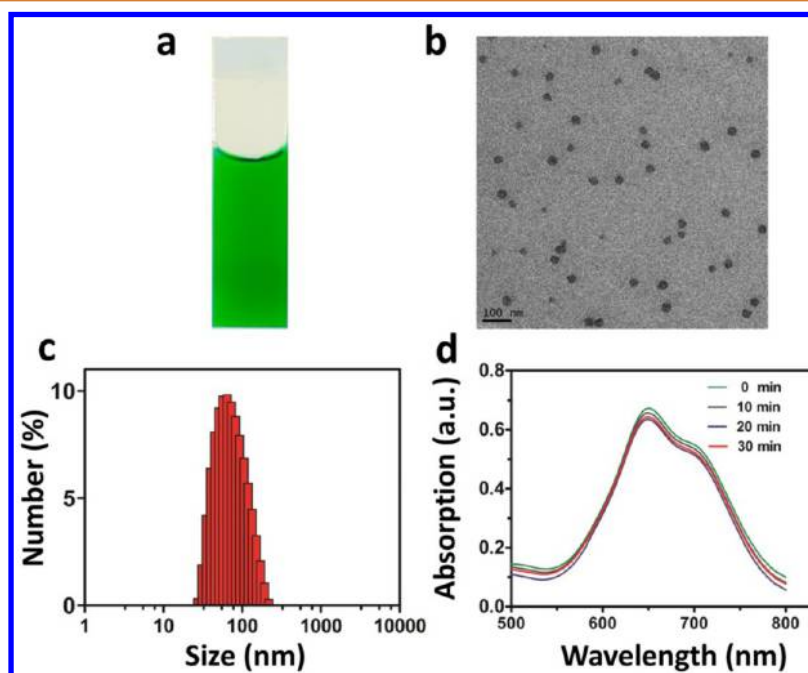


Figure 2. Characterization of physical and optical properties of cRGD-PDI NPs. (a) Picture of cRGD-PDI NPs in PBS (pH 7.4). (b) TEM and (c) DLS of cRGD-PDI NPs. (d) Photobleaching test: UV-vis-NIR absorption spectra of cRGD-PDI NP solution exposure under 700 nm laser irradiation (8 mJ cm^{-2}) for 0, 10, 20, and 30 min.

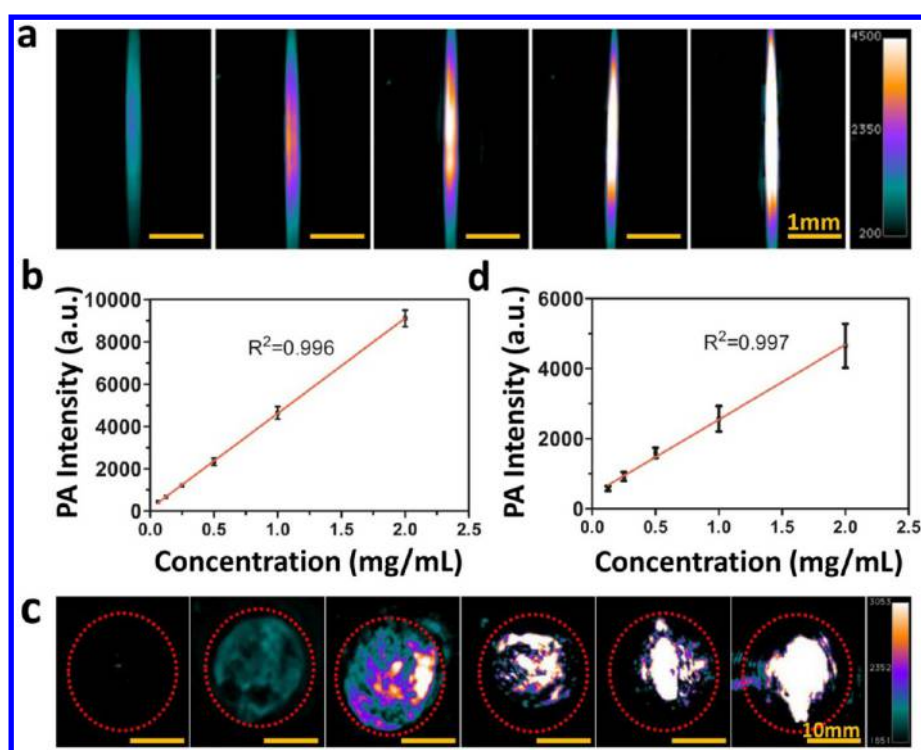


Figure 3. *In vitro* and *in vivo* study of PAI of cRGD-PDI NPs. (a) PAI of cRGD-PDI NPs in aqueous solution at concentrations of 0.125, 0.250, 0.500, 1.000, and 2.000 mg mL⁻¹, and (b) PA signal was observed to be linearly dependent on its concentration ($R^2 = 0.996$). All PAIs in (a) have the same scale bar. (c) PAI of cRGD-PDI NPs in living mice, which were injected subcutaneously (the depth is about 0.5 mm) at concentrations of 0.0625, 0.125, 0.250, 0.500, 1.000, and 2.000 mg mL⁻¹ (from left to right region enveloped by the red dotted line). (d) Linear regression for modeling the relationship between the PA signal and NP concentration is calculated on each inclusion ($R^2 = 0.997$). All PAIs in (c) have the same scale bar.

thrombus.^{43,44} In contrast to antibodies, the cRGD peptide is generally smaller in size and simpler in structure, causing less immunoreactivity.^{45,46} Thus, we hypothesized that the cRGD peptide modification of PDI NPs would specifically target GPIIb/IIIa to visualize early thrombus *in vivo* by PAI.

In this work, our designed cRGD-modified PDI (cRGD-PDI) NPs presented high PA intensity, good stability in light and serum, and a sufficient blood-circulating half-life. Furthermore, in comparison with an early thrombus test by cyclic Arg-Ala-Asp (cRAD) peptide-modified PDI NPs (cRAD-PDI NPs, no targeting ability to GPIIb/IIIa), blocking group, and old thrombus group, cRGD-PDI NPs exhibited excellent binding ability with GPIIb/IIIa and specifically lightened early thrombus in living mice by PAI. Meanwhile, cRGD-PDI NPs with PA contrast enhancement effectively provided the accurate information including the profile, size and conformation, and the spatial distribution of the thrombus, which can timely monitor the obstructive degree of thrombus in blood vessels and the therapy effect of thrombolysis.

RESULTS AND DISCUSSION

The preparation route of all PDI NPs and their usage for detecting early thrombus are illustrated in Figure 1. First, an amphiphilic PDI molecule was obtained by adding a long alkyl chain to one amide position of the PDI and a PEG chain with $M_w = 2000$ (PEG₂₀₀₀) to another amide position. The related synthetic route is shown in the Supporting Information, and the molecular structure was proven by ¹H NMR and MALDI-TOF MS in Figures S1–S12. The PDI NPs were then prepared by directly dissolving PDI molecules in water under the assistance

of sonication. The assembling number of PDI molecules per NP was calculated to be about 3.48×10^4 . The PDI NPs in water showed a dark green color (Figure 2a) and exhibited excellent water solubility of 10 mg mL⁻¹. cRGD and cRAD were then modified to the PEG surface of PDI NPs using sulfo-SMCC as a linker to investigate its thrombus-targeting ability. The obtained cRGD-PDI or cRAD-PDI NPs showed a relatively constant diameter of about 40.0 ± 3.1 and 41.2 ± 2.5 nm by transmission electron microscopy (TEM) (Figures 2b and S13). The dynamic light scattering (DLS) measurements also revealed that these NPs have a relatively narrow size distribution with a mean size of around 70.3 ± 2.3 and 68.9 ± 3.2 nm (Figures 2c and S13) in phosphate-buffered saline (PBS, 0.1 M, pH 7.4). The size of the PDI NPs observed under TEM is smaller than the DLS result due to their shrinking in the dry state. The ratio of non-cRGD-modified PEG (or non-cRAD-modified PEG) to cRGD-modified PEG (or cRAD-modified PEG) in a NP is calculated from MALDI-TOF MS to be about 2:1 (Figures S9 and S11), indicating a large amount of cRGD or cRAD (10k per NP) on the NP surface that can provide sufficient targeting ability. cRGD-PDI NPs exhibited NIR absorption in aqueous solution with a maximum absorption at 650 nm and a shoulder at 700 nm (Figure 2d). In this work, the wavelength at 700 nm was adopted as the NIR laser source for the PAI study. The extinction coefficient of PDI NPs at 700 nm was 2.58×10^8 M⁻¹ cm⁻¹, suggesting PDI NPs are excellent NIR light absorbers for PAI.

The cRGD-PDI and cRAD-PDI NPs can be stored in PBS (0.1 M, pH 7.4) without any precipitation for 12 months, more stable than the PDI NPs formed by the blending method which only remains for about 2 months.³⁸ When PDI NP aqueous

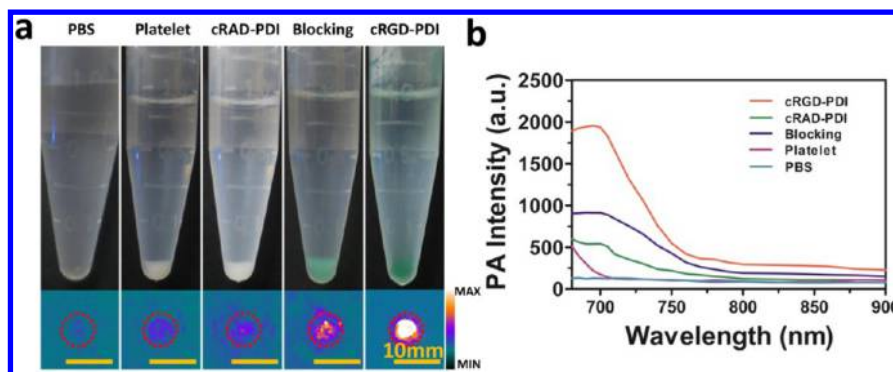


Figure 4. *In vitro* specificity binding assessment of cRGD-PDI NPs to activated platelets. (a) Pictures of activated platelets treated with PBS, pure platelets, activated platelets treated with cRAD-PDI NPs, activated platelets blocked by Eptifibatide and then treated with cRGD-PDI NPs, and activated platelets treated with cRGD-PDI NPs (from left to right in the top layer) and their respective PAIs (in bottom layer). All PAIs have the same scale bar. (b) PA spectra of those treated platelets.

solution (1 mg mL^{-1}) was diluted to 1000-fold, the NP size remained unchanged. Also, after incubation for 48 h in mouse serum at 37°C (Figure S14), the NP size in serum was slightly changed, indicating its potential good stability in blood. This prominent PDI NP stability can be attributed to the combined action of the strong π - π interaction among the planar PDI groups, the van der Waals' force from alkyl chains, and the hydrophobic interaction existing in one entity. The photostability of the cRGD-PDI NPs was further tested using a continuous laser irradiation at 700 nm and 8 mJ cm^{-2} and showed excellent photostability (almost no reduced absorption) during 30 min irradiation (Figure 2d). This photostability was derived from the PDI group, which has been proven to be more stable than the traditional organic dyes.³⁸ Therefore, the structure and optical stabilities gave cRGD-PDI NPs significant advantages for *in vivo* PAI.

The PA properties of the NPs were investigated *in vitro* with a phantom. Each EP tube with $10 \mu\text{L}$ of cRGD-PDI NPs at concentrations from 0.125 to 2.000 mg mL^{-1} was immersed in a tank filled water and subjected to PAI. The test results showed that the PA signal had good linear relationship with NP concentration ($R^2 = 0.996$, Figure 3a,b). To study the detection sensitivity of PA signals in a living body, $100 \mu\text{L}$ of cRGD-PDI NPs with different concentrations was mixed with matrigel and injected into the subcutaneous tissue of the lower back of the mouse. The PAI was analyzed (Figure 3c,d) and exhibited a linearly positive correlation between the PA signal intensity and dose concentration ($R^2 = 0.997$).

The targeting specificity of cRGD-PDI NPs to early thrombus was next evaluated *in vitro* in activated platelets. Each $100 \mu\text{L}$ platelet-rich plasma activated by $20 \mu\text{mol mL}^{-1}$ adenosine diphosphate (ADP) and $30 \mu\text{mol L}^{-1}$ thrombin receptor-activating peptide was incubated with cRGD-PDI NPs at 37°C for 60 min and then washed with PBS for further PAI. As a comparison, cRAD-PDI NPs, PBS, pure platelet aggregation, and the blocking group were also subjected to the same procedure. Figure 4a shows the visualized picture of all treated platelets. After treatment with the green cRGD-PDI NPs, the previous colorless platelets appeared green color while the PBS group still remained colorless, indicating the NPs were successfully adsorbed on the platelets. In addition, no color change of the platelet was observed after cRAD-PDI NP treatment, showing the existing targeting ability of cRGD-PDI NPs to the platelet aggregation. Considering that cRGD can efficiently bind to GPIIb/IIIa in early thrombus, the blocking

experiment was carried out to investigate its targeting specificity. After being blocked with Eptifibatide (a clinical application of the GPIIb/IIIa protein blocking agent) and then treated with cRGD-PDI NPs, an apparent decrease of the green color of platelets was observed, which manifested the targeting property of cRGD-PDI NPs to GPIIb/IIIa. PAI of all platelets in Figure 4a proved the feasibility of using cRGD-PDI NPs for targeted PAI of the thrombus. The PA signal intensity of activated platelets in the cRGD-PDI NP group was twice as strong as that in the blocking group and four times that of the cRAD-PDI NPs group. We further used PA spectra to differentiate the molecular signal of interest from the contrast or the background in the NIR region.⁴⁷ The PA spectra of the related platelets in Figure 4b showed that the maximum PA intensity peak of the cRGD-PDI group was at 700 nm , which was the same as cRGD-PDI NPs in aqueous solution, demonstrating that the enhanced PA signal in the platelet was derived from the targeted cRGD-PDI NPs.

We used MTT assay to evaluate the potential cytotoxicity of cRGD-PDI NPs on NIH3T3 cells. With the concentration of cRGD-PDI NPs ranging from 0 to $100 \mu\text{g mL}^{-1}$, all of the cells retained $>90\%$ viability, indicating their low cytotoxic effect (Figure S15). To study the blood circulation time of NPs, $300 \mu\text{L}$ of cRGD-PDI NPs at a concentration of 3.33 mg mL^{-1} was tail-vein-injected in normal mice ($n = 3$) for real-time detection by PAI. For quantitative comparison, an identical region of interest before and after cRGD-PDI NPs injection was selected. After 2 h injection of NPs, the intensity of the blood PA signal reached the maximum of 2-fold higher than that preinjection (3161 ± 97 versus 1066 ± 7 ; $p < 0.01$). The PA intensity then gradually decreased, and the intermediate half-life of cRGD-PDI NPs in blood was calculated to be about 22 h (Figure S16). Such a long circulating time of cRGD-PDI NPs can be explained by the PEG covering on the NP surface⁴⁸ and its appropriate NP size of around 70 nm ,⁴⁹ indicating its suitability for PAI application in blood vessels.

In vivo detection of early thrombus was performed on an FeCl_3 -induced murine model of jugular vein thrombus. Three wall-adherent thrombus mice were first subjected to US, MRI, and PAI to compare their thrombus imaging effects. In Figure 5a, in comparison with the normal jugular venous lumen, an ambiguous protrusion on the wall (in the white circled area), which belongs to the wall-adherent thrombus, was found in the lumen with early thrombus by US. In such, luminal blood appeared as black or dark gray and early thrombus as white-

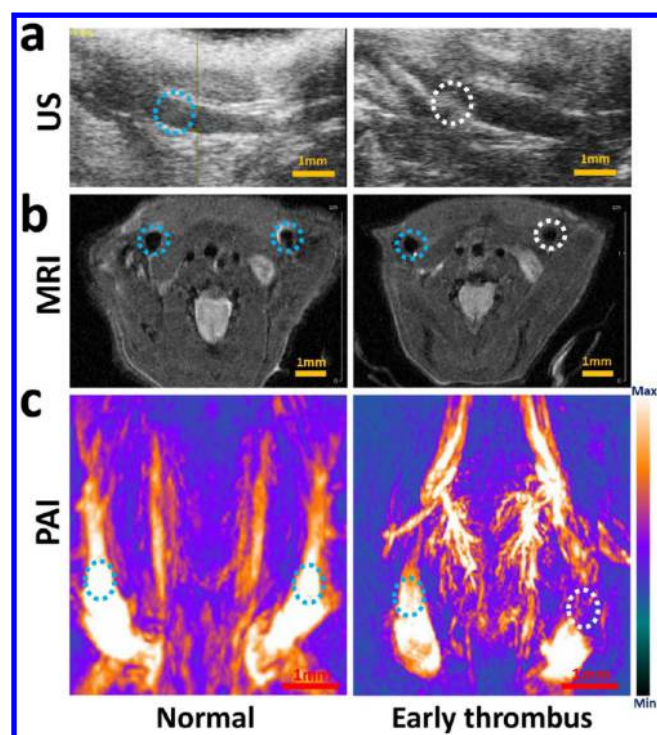


Figure 5. *In vivo* detection of early venous thrombus by MRI, US, and PAI. (a) US tests display the normal jugular venous lumen (in blue circle) and the lumen with early thrombus (in white circle). (b) Transverse sections (T_2 -weighted MRI, TR = 1206.9 ms, TE = 2.0 ms) of the normal jugular veins (in blue circle) and the vein with early thrombus (in white circle). (c) PAI showed normal jugular veins (in blue circle) and jugular veins with early thrombus (in white circle). Left pictures: normal mice. Right pictures: thrombus model. In the thrombus model, FeCl_3 -induced thrombus was only performed on the right jugular vein.

gray. However, it is really difficult to discern the thrombus from surrounding tissues by US due to its intrinsically poor contrast (the similar acoustic intensity of abnormalities with surrounding tissues).⁵⁰ In Figure 5b, we can easily visualize the jugular vein by T_2 -weighted MRI because MRI affords more detailed anatomic reference information and higher spatial resolution than US. However, consistent with the previous report, no clear evidence for thrombus formation by MRI was observed in the blood vessel having thrombus. The reason is that small and non-occlusive thrombus has only a minor impact on blood flow and may not give rise to a clear signal in MRI.⁵¹ PAI can provide good blood vessel imaging with high spatial resolution as well as high contrast owing to the significantly higher NIR absorption of hemoglobin in blood than in surrounding tissues.⁵² In Figure 5c, the morphology and distribution of the blood vessel, even the smaller vessel, can be clearly discerned by PAI. Different with the normal vessel in the blue circled area, the vessel with thrombus was clearly observed with a loss of PA signal in the white circled area. It indicates the existence of thrombus in this location because ischemia (lacking hemoglobin) in the thrombus region resulted in the reduced PA signal of blood.^{15,16} Compared to MRI and US, it is obvious that the thrombus formation can be unambiguously observed by PAI, demonstrating that PAI is promising for thrombus detection. However, owing the signal-off effect of PAI on thrombus, lightening thrombus by a PA contrast agent is

therefore more significant for obtaining detailed information on thrombus.

Subsequently, *in vivo* PAI of early thrombus by cRGD-PDI NPs was performed. One group of three wall-adherent thrombus mice were tail-vein-injected with 300 μL of cRGD-PDI NPs at a concentration of 3.33 mg mL^{-1} , and the other two groups were injected with cRAD-PDI NPs and PBS as control groups. The PAI of each experimental group in every time point was visualized in Figure 6a. All PAIs of the three groups before NP injection revealed obvious PA signals of the normal vessels in the blue circled area and the signal-off effect in thrombus regions (in the white circled area). After 2 h injection of cRGD-PDI NPs, part of the thrombus region in the white circle area started to appear with an increased PA signal. Almost the whole thrombus region showed obviously increased PA signal after 6 h injection (Figure 6a,b) and the PA intensity reached the maximum (4536 ± 121) after 24 h injection, which was 4.3-fold higher than that before NP injection (Figure 6c). After 48 h injection of cRGD-PDI NPs, the enhanced PA signal in thrombus was more clearly visible. The localization of cRGD-PDI NPs in the thrombus was further confirmed by PA spectra measurements. In Figure 6c, the thrombus region *in vivo* exhibited a strong peak of PA signal at 700 nm after 12 h NP injection. This PA peak position is consistent with the characteristic PA peak of cRGD-PDI NPs in aqueous solution, much different from that injected with PBS, demonstrating the accumulation of cRGD-PDI NPs in the thrombus. Thus, the successful lightening of the thrombus by cRGD-PDI NPs displayed sufficient binding capability to thrombus *in vivo*. In contrast, no enhanced PA signal was found in the thrombus region of mice injected with cRAD-PDI NPs and PBS. In Figure 6b, a significantly increased PA intensity occurred in the thrombus region of the cRGD-PDI NP group compared with that of the cRAD-PDI NP control group after 6 h injection (2287 ± 69 versus 1183 ± 27 , $p < 0.01$) and reached the highest at 3.5-fold after 24 h injection. This result exhibited the good targeting ability of cRGD-PDI to early thrombus, which may contribute to its strong binding ability to GPIIb/IIIa on activated platelets in early thrombus. To prove this, a GPIIb/IIIa blocking test was applied *in vivo*. GPIIb/IIIa blocking agent Eptifibatid and cRGD-PDI NPs were injected in sequence *via* tail vein within 1 h. It was found that the signal area in the thrombus was completely suppressed at each time point. These findings manifested that the greatly enhanced PA signal of jugular vein thrombus was caused by cRGD-PDI NPs binding to GPIIb/IIIa in the venous thrombus *in vivo*.

Further analysis showed that after PDI NP injection, the PAIs of the normal vessels (Figure 6a, dotted by blue line in the square) in cRGD-PDI NP and cRAD-PDI NP groups both became the brightest at 2 h and then gradually decreased, which is in accordance with the PDI NPs in normal mice. However, it is intriguing to find that the blood signal intensity at the thrombus side (Figure 6a, dotted by white line in the square) in both groups reached the maximum at 12 h, much longer than that of the control vessel (Figure 6d). The observed prolonged retention time of cRGD-PDI NPs close to thrombus is mainly due to the temporary stasis of blood where the thrombus delayed the blood flow and subsequently afforded higher accumulation of cRGD-PDI NPs in the local blood region (Figure 6e).⁴¹ Therefore, based on this phenomenon, we may understand the obstructive degree of thrombus through investigation of the retention time of NPs in the blood vessels around the thrombus by PAI. To evaluate the feasibility of

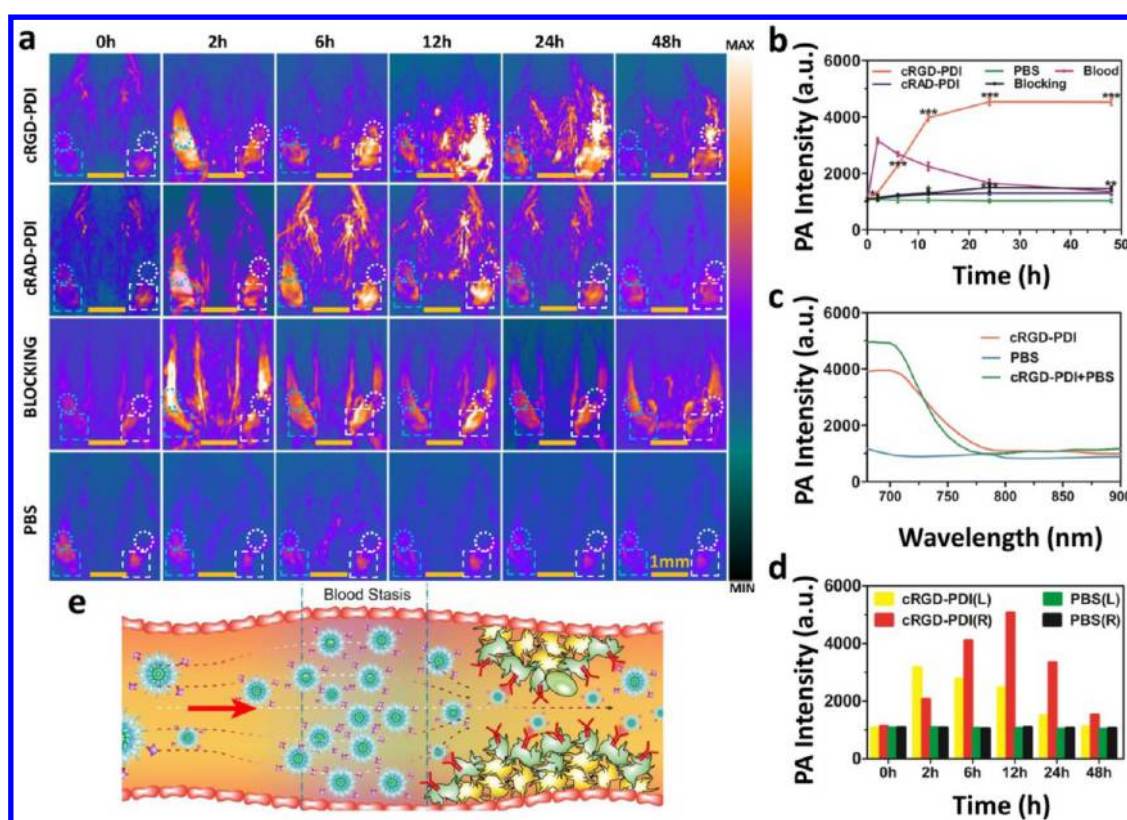


Figure 6. *In vivo* PA detection of early thrombus. (a) PAI of the mouse jugular veins with early thrombus of the cRGD-PDI NPs group, cRAD-PDI NPs group, blocking group, and PBS control group at different treatment time. For analysis of the PAI effect of early thrombus, PA intensity of the blood vessel with early thrombus (the circle region enveloped by the white dotted line) was compared with that of the normal vessel region in the control side (the circled region enveloped by the blue dotted line). To study the obstructive degree of early thrombus, PA intensity of the blood close to the thrombus (the square region enveloped by the blue dotted line) was also compared with that of the blood in normal vessel (the square region enveloped by the white dotted line in (a)) of the cRGD-PDI NPs group, cRAD-PDI NPs group, blocking group, and PBS control group and the blood in normal vessels (the circle region enveloped by the blue dotted line of the cRGD-PDI NPs group in (a)) with injection time. (b) Change of PA intensity in the thrombus (the circle region enveloped by the white dotted line in (a)) of the cRGD-PDI NPs group, cRAD-PDI NPs group, blocking group, and PBS control group and the blood in normal vessels (the circle region enveloped by the blue dotted line of the cRGD-PDI NPs group in (a)) with injection time. (c) PA spectra of cRGD-PDI NPs (1 mg mL^{-1}) in PBS (the green curve) and thrombus after 12 h injection of PBS (the blue curve) and cRGD-PDI NPs (the red curve) *in vivo*. (d) Change of PA intensity of blood close to the thrombus (the square region enveloped by the white dotted line in (a)) and blood in normal vessels (the square region enveloped by the green dotted line in (a)) with injection time in the cRGD-PDI NP group and PBS control group. In (d), cRGD-PDI (L) refers to the normal vessel (left vein) and cRGD-PDI (R) refers to the vessel with thrombus (right vein) in PAI of the cRGD-PDI NPs group. PBS (L) refers to the normal vessel (left vein), and PBS (R) refers to the vessel with thrombus (right vein) in PAI of the PBS group. It was shown that the retention time of cRGD-PDI NPs in the blood vessel close to the thrombus region was prolonged. (e) Illustration of the mechanism of the prolonged retention time of cRGD-PDI NPs in the blood vessel close to the thrombus region.

cRGD-PDI NPs as a PA contrast agent for obtaining accurate information on early thrombus, we also obtained PAI under 850 nm laser irradiation (no light absorption of cRGD-PDI NPs at this wavelength) and compared it with PAI under 700 nm laser irradiation. In Figure S17, after injection of NPs, PAI under 850 nm laser irradiation only showed the background signals. Almost no signal changed, and the loss of PA signal in thrombus (in the yellow circle area) existed in the whole observation period. Combined with PAI under 700 nm laser irradiation that exhibited the enhanced PA signal of NPs in the same position (in the white circle area), we can unambiguously distinguish thrombus from the surroundings. Furthermore, due to the enhanced PA signal in early thrombus after injection of cRGD-PDI NPs and the excellent 3D characteristics of PAI, the amplified PA brightness allowed us to achieve a flexible 3D signal reconstruction to better delineate early thrombus in detail, including its profile, size, and conformation, compared to those of PAI without cRGD-PDI NP injection (Figure 7). The flexibility to rotate, scale, and view the interesting region from

various orientations can facilitate visualized diagnostics of early thrombus. In this experiment, a $0.5 \text{ mm} \times 0.2 \text{ mm}$ micro-thrombus was easily observed by PAI. Furthermore, considering that the spatial resolution of our PA instrument (Endra Nexus 128 PA tomography system) is $<0.2 \text{ mm}$, it is possible that a smaller thrombus can be detected by PAI.

In order to minimize the interference of the PA signal from surrounding tissue and further test the PAI capability of cRGD-PDI NPs on venous thrombus, the *ex vivo* PA data of the jugular vein thrombus were collected. After excising and embedding thrombus in agarose gel, the *ex vivo* PAI was compared with the *in vivo* imaging. In Figure 8a,b, the *ex vivo* PAI of the cRGD-PDI NP group clearly exhibited the enhanced PA signals, and their PA signal change with time was consistent with the living imaging, indicating the accumulation of cRGD-PDI NPs in the jugular vein thrombus. Instead, there was almost no PA signal in the jugular vein thrombus injected with cRAD-PDI NPs, demonstrating the good targeting capability of cRGD-PDI NPs to thrombus. Next, the corresponding result of

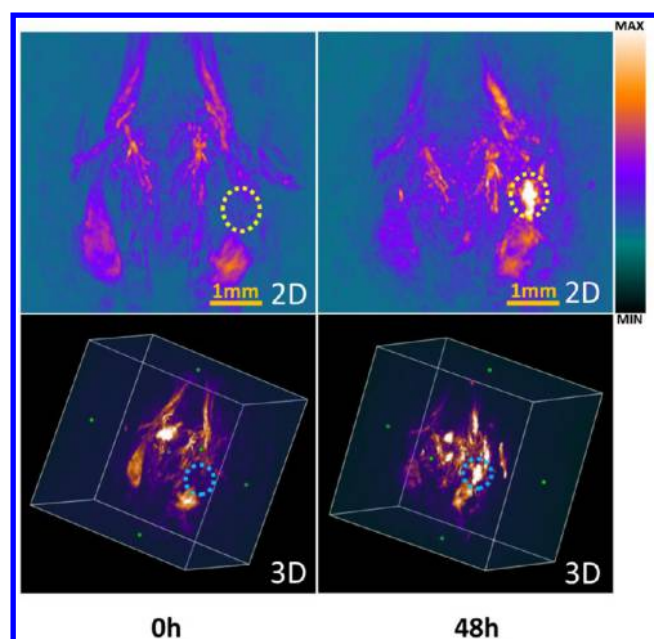


Figure 7. PAI of early thrombus (region enveloped by the yellow dotted line in the 2D picture and blue dotted line in the 3D picture) 0 h and after 48 h injection of cRGD-PDI NPs.

immunohistochemistry showed that GPIIb/IIIa was expressed abundantly in the luminal thrombus of the test group, less in the blocked thrombus, and seldom in the control jugular vein, which clearly proved the specificity of cRGD-PDI NPs binding to GPIIb/IIIa on the activated platelets in early thrombus (Figure 8c and 8d).

Due to the targeting ability of cRGD-PDI NPs to GPIIb/IIIa and slight GPIIb/IIIa expression in old thrombus, we thus tested the feasibility of cRGD-PDI NPs to distinguish early thrombus from old thrombus *in vivo*. The ferric-chloride-induced acute jugular venous thrombus after 3 days of injury was adopted as the old thrombus model. Similar to early thrombus, old thrombus also exhibited the signal-off effect before NP injection (Figure 9a), indicating its ineffectiveness for PAI to clarify the thrombus status without using the PA contrast agent. When cRGD-PDI NPs (3.33 mg mL^{-1} , 0.3 mL) as a contrast agent were tail-vein-injected for PAI, we found that in contrast to the enhanced PA signal (4536 ± 121) in the early thrombus (Figure 6a), no enhanced PA signal (1056 ± 96) was observed in the old thrombus region during 48 h after NP injection (Figure 9a). Thus, early thrombus can be easily differentiated from old thrombus through observation of the PA signal variation in the thrombus region with time after injection of cRGD-PDI NPs. Subsequently, the old thrombus was resected and stained with anti-CD41, and only a small amount of GPIIb/IIIa expression was found (Figure 9b).⁵³ A similar result was also reported in the ultrasound diagnosis of early thrombus using cRGD-modified liposomes.¹⁰ The most likely reason is that integrin GPIIb/IIIa exposes new epitopes and binding sites (ligand-induced binding sites) on the surface of activated platelets in early thrombus, where RGD, not RAD, can recognize and combine. However, the configuration of high-affinity GPIIb/IIIa that was not combined will change to a low-affinity or rest state again as early thrombus grows into old thrombus.⁵⁴ Therefore, the GPIIb/IIIa-targeted cRGD-PDI NPs can provide an opportunity to distinguish early thrombus from old thrombus. Because such a lightening effect from cRGD-PDI NPs can display the detailed information on early

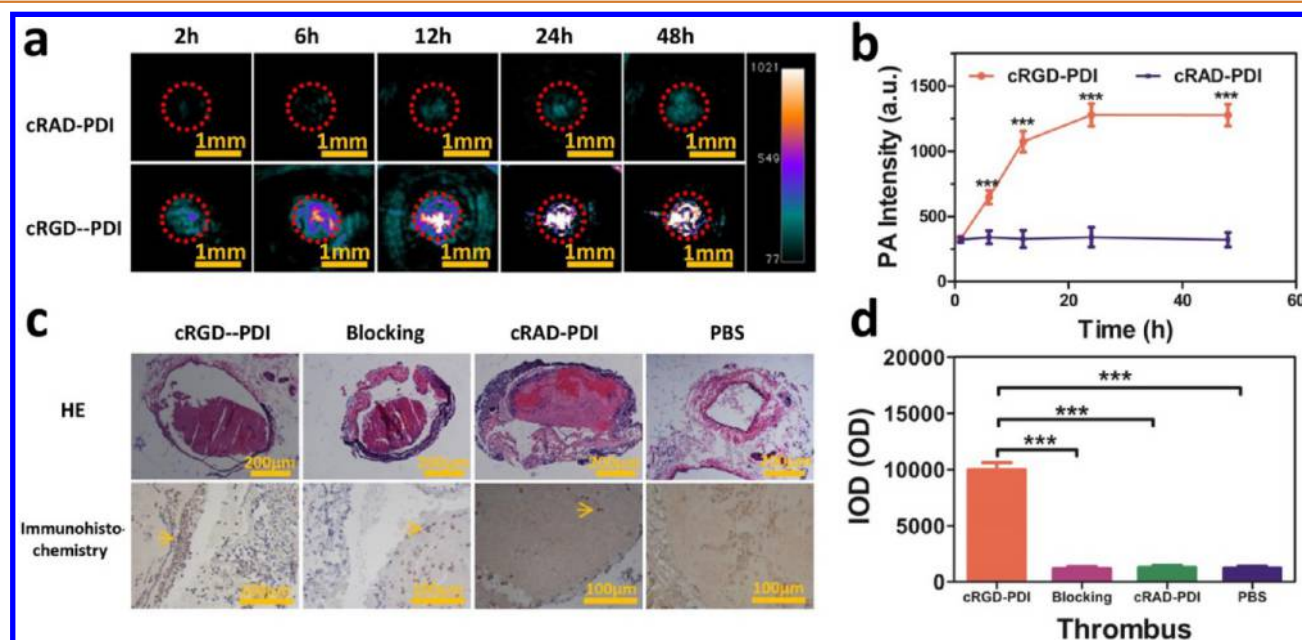


Figure 8. *Ex vivo* specificity binding assessment of cRGD-PDI NPs to early thrombus. (a) *Ex vivo* PAI of excised thrombus after systemic administration of cRGD-PDI and cRAD-PDI ($300 \mu\text{L}$, 3.33 mg mL^{-1}) from 2 to 48 h. (b) Relationship of the PA signal intensity at 700 nm (region enveloped by the red dotted line in (a)) with time after injection of cRGD-PDI NP and cRAD-PDI NPs. (c) Presence of platelet-containing wall-adherent thrombosis in the 5% FeCl_3 -applied jugular veins partially occluded the total vessel lumen by pathological examination in the top row. Corresponding expression of GPIIb/IIIa (yellow arrows depict the typical appearance) in the thrombus was also observed through immunohistochemistry in the bottom row. The PBS group was a negative control. (d) Plot of GPIIb/IIIa density in each group according to the integrated optical density (IOD), determined by Image-Pro Plus software, in the thrombus of five representative sections of each group. Error bars were based on standard error of mean (SEM) ($*p < 0.05$, $**p < 0.01$, $***p < 0.001$, $n = 3$).

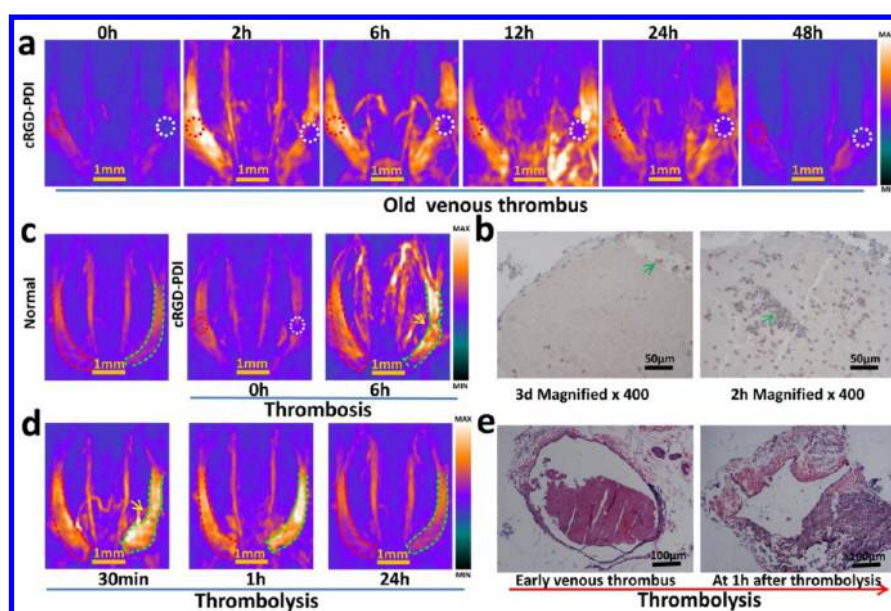


Figure 9. Distinguishing early thrombus from old thrombus by PAI after injection of cRGD-PDI NPs and its potential applications of monitoring the thrombolysis effect. (a) PAI of old venous thrombus (3 days after injury) showing that no PA signal was enhanced in the old thrombus (region enveloped by the white dotted line) after injection of cRGD-PDI NPs. (b) Corresponding expression of GPIIb/IIIa (stained with anti-CD41) in old thrombus was very small (indicated by the green arrow in the left picture) through immunohistochemistry, in comparison with the abundant GPIIb/IIIa in early thrombus (indicated by the green arrow in the right picture). (c) PAI of normal jugular veins before FeCl_3 treatment (left), and FeCl_3 -treated vein after injection of cRGD-PDI NPs at 0 h (middle) and 6 h (right). After 6 h injection of cRGD-PDI NPs ($300 \mu\text{L}$, 3.33 mg mL^{-1}), the PA intensity of early thrombus increased compared with that at 0 h (region enveloped by the white dotted line), and the margin of blood vessels at the thrombus region (displayed by green arc line) was irregular. (d) PAI of jugular veins with early thrombus, which was first treated with cRGD-PDI NPs for 6 h and then treated with urokinase for thrombolysis. After 1 h intravenous application of urokinase, the profile of the right jugular vein with thrombus completely became smooth (displayed by green arc line). After 24 h thrombolysis, the PA signal intensity and the morphology of normal vessels (displayed by red arc line) and vessel with thrombus (displayed by green arc line) were similar to each other. (e) Histology demonstrated the formation of wall-adherent non-occlusive thrombosis after FeCl_3 treatment and the disappearance of thrombus after 1 h thrombolysis.

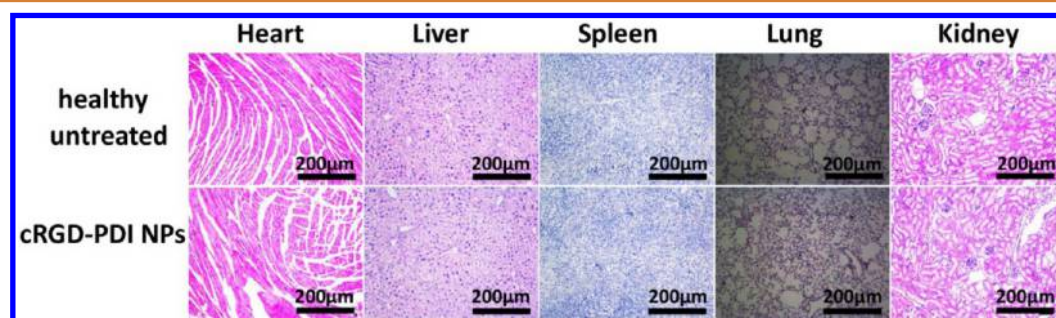


Figure 10. Toxicity evaluation of cRGD-PDI NPs. Micrographs of H&E-stained organ slices from untreated mice (top row) and 7 days after treatment (bottom row) with cRGD-PDI NPs. Examined organs included heart, liver, spleen, lungs, and kidneys. No obvious change in cellular structure was observed for the treated group.

thrombus, it was considered that the lightening effect can also be used to monitor the thrombolytic process. Consequently, the monitoring ability of cRGD-PDI NPs for the therapeutic effect of thrombolysis on early thrombus was investigated. In this experiment, cRGD-PDI NPs were first injected into the vein until an enhanced PA signal in the thrombus region was observed after 6 h injection (Figure 9c). Then 50 000 international units (IU) of human urokinase (thrombolytic agents) was injected *via* the tail vein for thrombolytic therapy. After 6 h NP injection, the vessel around the lightened thrombus showed an irregular margin in the PAI. The related profile gradually became smooth only after 30 min injection of thrombolytic agents and became similar to the normal vessel after 1 h injection (Figure 9d). This phenomenon indicates the

successful removal of the thrombus and the fast vein recanalization after drug administration. Different than the remaining strong PA signal of untreated early thrombus after 48 h NP injection, the weakened PA signal after thrombolytic therapy was nearly the same as that in the normal vessel, also representing the successful thrombolysis. Combined with the visual disappearance of early thrombus after 1 h thrombolytic therapy through the *ex vivo* thrombus resection (Figure 9d), all of the results strongly proved the feasibility of using PAI for timely monitoring of thrombolysis.

The cRGD-PDI NP metabolism biodistribution at 2 days was studied by *ex vivo* PAI of resected internal organs (Figure S18a, Supporting Information). The biodistribution in the healthy untreated mice and injected with cRAD-PDI NPs was also

analyzed for comparison. It was found that a very weak PA signal was present in all organs of the untreated mice. However, for the mice injected with cRGD-PDI NPs and cRAD-PDI NPs, the NPs exhibited significant uptake in the liver and spleen but little in the muscle, stomach, intestine, heart, and kidney. Almost no NP accumulation appeared in the bone and skin (Figure S18b, Supporting Information). Such a distribution pattern is in agreement with a NP size greater than 10 nm, which is mainly cleared through the reticuloendothelial system (primarily through liver and spleen).⁵⁵ We further preliminarily evaluated the *in vivo* toxicity of cRGD-PDI NPs in mice through H&E staining of major organs after 7 days of NP injection. H&E staining of liver, spleen, and kidney, in which PDI NPs accumulated, showed no apparent damage to the cellular structures. Also, there was no obvious inflammation of major organs (Figure 10), suggesting the favorable biocompatibility and low cytotoxicity of cRGD-PDI NPs. Further investigations are still needed to comprehensively evaluate its long-term toxicity.

CONCLUSION

In summary, we developed organic NPs assembled by amphiphilic PDI macromolecules for efficiently lightening early thrombus *in vivo* by PAI. The as-prepared cRGD-PDI NPs possessed special properties with high PA intensity, high biocompatibility and photostability, and high affinity for the GPIIb/IIIa receptor on activated platelets, thereby distinguishing early thrombus from old thrombus. Furthermore, the PDI NP-based contrast agent presented good PA signal for profiling the edge of the thrombus and consequently for monitoring the thrombolytic therapy. Overall, our work provides insight on how to design or select suitable organic NP-based contrast agents for promoting the development of PAI technology for accurate diagnosis of early thrombus.

EXPERIMENTAL SECTION

The synthetic routes to the PA agents are shown in the Supporting Information.

Chemicals. tBOC-NH-poly(ethylene glycol)-NH₂ with a molecular weight of 2 kDa was purchased from Laysan Bio, Inc., and 3,4,9,10-perylenetetra-carboxylic dianhydride, 2-*n*-octyl-1-dodecylamine, *N*-methyl-2-pyrrolidinone, pyrrolidine, isopropyl alcohol, trifluoroacetic acid, succinimidyl 4-(*N*-maleimidomethyl) cyclohexane-1-carboxylate, and cRGDFc were purchased from Sigma-Aldrich.

Material Characterization. TEM images were obtained on a JEOL TEM 2010 electron microscope at an acceleration voltage of 100 kV. Dynamic light scattering was performed on the 90 Plus particle size analyzer (Brookhaven Instruments). NMR spectra were recorded on a Bruker Ultra Shield Plus 400 MHz NMR (¹H, 400 MHz; ¹³C, 100 MHz). The matrix-assisted laser desorption/ionization time-of-flight mass spectroscopy (MALDI-TOF MS) measurements were carried out with a Shimadzu AXIMA-CFR mass spectrometer. UV-visible absorption spectra were recorded on a PerkinElmer Lambda 35.

Preparation of PDI NPs. Detailed synthesis and characterization of cRGD-PDI NPs and cRAD-PDI NPs is described in the Supporting Information. Briefly, PDI NPs in aqueous solution were prepared by directly adding amphiphilic PDI (10 mg) into 1 mL of water under ultrasonication for 5 min at room temperature. The obtained PDI NPs were surface-modified with cRGD and cRAD. The final cRGD-PDI NPs and cRAD-PDI NPs were reconstituted in PBS and filtered through a 0.22 μm filter for cell and animal experiments. The density of cRGD or cRAD on the surface of cRGD-PDI NPs or cRAD-PDI NPs was calculated by MALDI-TOF MS.

Cytotoxicity Assay. NIH/3T3 fibroblast cells were cultured in Dulbecco's modified Eagle medium (DMEM) having 1% penicillin–

streptomycin and 10% fetal bovine serum (FBS) at 37 °C in a humidified environment with 5% CO₂. MTT (3-(4,5-dimethylthiazol-2-yl)-2,5-diphenyl tetrazolium bromide) assay was applied to evaluate the NP cytotoxicity. In brief, the murine fibroblast NIH-3T3 cells at a concentration of 4 × 10⁴ cells mL⁻¹ in medium were incubated in a 96-well plate. After 24 h incubation, the cells were further incubated with cRGD-PDI NPs with different concentrations (0–1000 μg mL⁻¹) for 24 and 48 h. MTT compounds were further added to the medium for another 3 h incubation. Cell viability was then evaluated by investigating absorbance at 540 nm and using absorbance at 650 nm as a reference. All samples were used in triplicate, and the related experiments were all replicated three times.

PA Instrumentation. In this experiment, the Endra Nexus 128 PA tomography system (Endra, Inc., Ann Arbor, MI) was applied for PAI. The instrument has a tunable nanosecond pulsed laser (wavelength range = 650–950 nm, 7 ns pulses, 20 Hz pulse repetition frequency, 9 mJ pulse⁻¹ on the animal surface) and 128 unfocused ultrasound transducers (5 MHz center frequency, 3 mm diameter) arranged in a hemispherical bowl.

Mouse Model of FeCl₃-Induced Non-occlusive VTE in the Jugular Vein. All surgical procedures and post-operative care were performed in accordance with institutional guidelines on animal care. Male C57BL/6 mice (body weight = 25–30 g, age = 8–12 weeks) were anesthetized by using a mixture of intraperitoneal ketamine/xylazine. Before making the model, the hair on each mouse's neck was removed with hair remover lotion. The right main jugular vein was exposed by blunt dissection from circumferential connective tissues. Subsequently, a filter paper (1 × 2 mm) soaked with 5% FeCl₃ was placed on top of the vessel and incubated for 5 min. To ensure that the location of the FeCl₃ was only placed on top of the vessel surface, two stretches of parafilm were placed on both sides of the vessel. After removal of the filter paper, the vessel was washed with 0.9% NaCl to remove residual FeCl₃. As a sham control, the left jugular vein was surgically exposed and soaked with PBS. The presence of non-occlusive thrombus in the right jugular vein was confirmed by histology.

In Vitro PAI of Activated Platelets. Fresh citrated blood was obtained from healthy human volunteers. Platelet-rich plasma (PRP) was obtained *via* centrifugation of whole blood at 800g for 15 min. This experiment was divided into four groups. Each EP tube was added with 100 μL of PRP, which was activated with 20 μmol mL⁻¹ ADP and 30 μmol L⁻¹ thrombin-receptor-activating peptide before incubation with cRGD-PDI, cRAD-PDI, PBS at 37 °C for 60 min, and then centrifuged at 12 000g for 15 min to obtain platelet precipitates. After 100 μL of PBS was added, the platelet precipitate was centrifuged at 12 000g for 5 min with ultrasonic vibration, extensively washed with PBS three times, and then subjected to a scan of PA spectra at excited wavelengths ranging from 680 to 950 nm with a step of 5 nm. To demonstrate the specificity of cRGD-PDI NPs to GPIIb/IIIa receptor *ex vivo*, a competitive inhibition experiment was adopted. One hundred microliters of Eptifibatid (Integrilin), a GPIIb/IIIa antagonist commonly used in clinical practice, was added to the activated PRP to saturate GPIIb/IIIa before incubation with cRGD-PDI NPs. The specificity of cRGD-PDI NP-targeting activated platelets was analyzed using PAI. Under each condition, the same experiments were performed three times.

In Vivo US and MRI. After non-occlusive thrombosis was induced with FeCl₃ as described above, mice (*n* = 3) were subjected to ultrasonographic imaging (Vevo 2100, VisualSonics Inc., Toronto, Canada). Mice were anesthetized and maintained with isoflurane anesthesia (1.5–2%) and laid on a platform in the supine position with all legs taped to electrocardiogram (ECG) electrodes for heart rate monitoring. A 30 MHz probe was used to gather venous thrombus information.

After US detections, MRI was performed with a 7.0 T Micro-MR (Bruker, Rheinstetten, Germany). Mice were further anesthetized and maintained with isoflurane anesthesia (1.5–2%) and were connected to an ECG and breathing monitor and kept at 37 °C in the animal bed. Imaging consisted of a pilot scan with two orthogonal slices followed by a respiration-gated coronal two-dimensional gradient-echo

sequence oriented vertical to the esophagus with an echo time (TE) of 2.0 ms, a repetition time (TR) of 1206.9 ms, a flip angle of 180°, and a field of view of 25 × 25 mm. Data were gathered with a 25 mm resonator tunable to T_2 -weighted ^1H MRI.

In Vivo and Ex Vivo PAI. Mice were randomly assigned to cRGD-PDI, cRAD-PDI, and PBS groups ($n = 3$ for each group) before PAI was performed. After the non-occlusive thrombus was induced with FeCl_3 as described above, mice were tail-vein-injected (15 min after the end of the surgical procedures) with either the cRGD-PDI or cRAD-PDI NPs (3.33 mg mL^{-1}) in a total volume of 0.3 mL. The group injected with 0.3 mL of PBS was also used as the control group. Anesthesia was induced with 5% and maintained with 1–2% isoflurane during the PAI experiment. Except for the nose and mouth, the neck of mouse was immersed in a water tank with a transparent window at the bottom to let NIR light penetrate underneath to the prone position. Then the bilateral jugular veins were simultaneously imaged at 2, 6, 12, 24, and 48 h after injection of the probes. A competitive inhibition experiment was applied on three mice with thrombus to prove the binding ability of cRGD-PDI NPs to GPIIb/IIIa *in vivo*. Eptifibatid ($1.8 \mu\text{g g}^{-1}$) was injected to saturate GPIIb/IIIa before NP administration. cRGD-PDI NPs were then injected, and PAI was obtained according to the above-mentioned procedure. After *in vivo* imaging, the mice were euthanized. Their jugular veins were excised, embedded in agarose gel, and subjected to PAI at various time points. For clearance biodistribution experiment of cRGD-PDI NPs, mice ($n = 3$) were euthanized 7 days after injection of the contrast agent. Transcardiac perfusions through the left ventricle were then performed with PBS to remove the residual blood. After that, all organs were harvested, embedded in agarose gel, and subjected to PAI under 700 nm laser irradiation.

To study the capability of cRGD-PDI NPs on monitoring thrombolysis effect *in vivo*, we performed thrombolysis in a group ($n = 3$) of FeCl_3 -induced non-occlusive VTE in the jugular vein by injection of human urokinase (Medac, Wedel, Germany). After the enhanced PA signal was observed in thrombus after 6 h injection of cRGD-PDI NPs, 300 μL of urokinase (50 000 IU) was tail-vein-injected and PAI was then performed after 30 min, 1 h, and 24 h. When *in vivo* PAI was finished, the jugular veins were excised and stained with hematoxylin and eosin to confirm the success or failure of thrombolysis.

To evaluate whether cRGD-PDI NPs can be used to detect old thrombus, FeCl_3 -induced acute jugular venous thrombus after 3 days of injury was adopted as the old thrombus model. cRGD-PDI NPs (3.33 mg mL^{-1} , 0.3 mL) were injected *via* tail vein in mice with the old thrombus model ($n = 3$) and then transferred to the PAI system. After 48 h PAI, those mice were killed and jugular veins were removed. Then the tissue was stained for GPIIb/IIIa analysis as described in Supporting Information.

Histopathology and Immunohistochemistry. After *in vivo* PAI was finished, animals were anesthetized with ketamine and xylazine. Transcardiac perfusions were carried out with saline and 4% paraformaldehyde. The jugular veins were excised, fixed in formalin, and embedded in paraffin. Serial 4 μm thick cross sections were stained with hematoxylin and eosin to confirm the formation of non-occlusive thrombus in the right jugular vein. In immunohistochemistry, GPIIb/IIIa was detected with rat anti-mouse GPIIb polyclonal antibody (Clone MWReg30, Abcam, Inc., America), and then primary antibody was detected with a goat anti-rat antibody (HRP, Abcam, Inc., America). All sections were immunostained with horseradish peroxidase substrate solution ($\text{DAB} + \text{H}_2\text{O}_2$ in distilled water) and then counterstained with hematoxylin. For each group, five representative sections were used, and the integrated optical density was semiquantified by Image-Pro Plus software.

Statistical Methods. The data of PA signal intensities in regions of interest were analyzed by the OsiriX imaging system software package. All data were given as mean \pm SD. The statistical calculations were carried out by GraphPad Prism v.5 (GraphPad Software, Inc., La Jolla, CA). Correlation coefficients were concluded by using linear regression and calculating Pearson correlation coefficient (r). In this study, statistical comparisons between various groups were imple-

mented with two-way analysis of variance. The comparison of PAI intensity between the two time points of the same group was performed with a paired t test; $p < 0.05$ was considered to be statistically significant.

ASSOCIATED CONTENT

Supporting Information

The Supporting Information is available free of charge on the ACS Publications website at DOI: 10.1021/acsnano.7b00594.

Details of the synthetic route (Scheme S1) and characterization (Figures S1–S12) of PDI NPs; representative TEM images and DLS of cRAD-PDI NPs (Figure S13); stability of cRGD-PDI NPs in serum (Figure S14); cellular toxicity evaluation of cRGD-PDI NPs (Figure S15); PA intensity changes of blood in normal mice after injection of PDI NPs (Figure S16); *in vivo* PA detection of early thrombus under laser irradiation at different wavelengths (Figure S17); and *ex vivo* PA investigation of major organs (Figure S18) (PDF)

AUTHOR INFORMATION

Corresponding Authors

*E-mail: yuaxi@whu.edu.cn.

*E-mail: iamqlfan@njupt.edu.cn.

ORCID

Zhen Yang: 0000-0003-4056-0347

Quli Fan: 0000-0002-9387-0165

Author Contributions

[§]C.C. and Z.Y. contributed equally to this work.

Notes

The authors declare no competing financial interest.

ACKNOWLEDGMENTS

This work was financially supported by the National Natural Science Foundation of China (Nos. 21674048, 21574064, 61378081, and 81501535), the Natural Science Foundation of Jiangsu Province of China (Nos. NY211003 and BM2012010), International Cooperation Project of Hubei Province (2015BHE018), Hubei Province's Outstanding Medical Academic Leader Program, Wuhan's Huanghe Talents Program, and Zhongnan Hospital of Wuhan University Science, Technology and Innovation Seed Fund (cpxy20160045).

REFERENCES

- (1) Go, A. S.; Mozaffarian, D.; Roger, V. L.; Benjamin, E. J.; Berry, J. D.; Blaha, M. J.; Dai, S.; Ford, E. S.; Fox, C. S.; Franco, S.; Fullerton, H. J.; Gillespie, C.; Hailpern, S. M.; Heit, J. A.; Howard, V. J.; Huffman, M. D.; Judd, S. E.; Kissela, B. M.; Kittner, S. J.; Lackland, D. T.; et al. A Report from the American Heart Association. *Circulation* **2014**, *129*, 399–410.
- (2) Heit, J. A.; Spencer, F. A.; White, R. H. The Epidemiology of Venous Thromboembolism. *J. Thromb. Thrombolysis* **2016**, *41*, 3–14.
- (3) Heit, J. A. Epidemiology of Venous Thromboembolism. *Nat. Rev. Cardiol.* **2015**, *12*, 464–474.
- (4) Lecumberri, R.; Alfonso, A.; Jimenez, D.; Fernandez Capitan, C.; Prandoni, P.; Wells, P. S.; Vidal, G.; Barillari, G.; Monreal, M. Dynamics of Case-Fatality Rates of Recurrent Thromboembolism and Major Bleeding in Patients Treated for Venous Thromboembolism. *Thromb. Haemostasis* **2013**, *110*, 834–843.
- (5) Landman, G. W.; Gans, R. O. Oral Rivaroxaban for Symptomatic Venous Thromboembolism. *N. Engl. J. Med.* **2011**, *364*, 1178.

- (6) Perrier, A.; Roy, P. M.; Aujesky, D.; Chagnon, I.; Howarth, N.; Gourdiere, A. L.; Leftheriotis, G.; Barghouth, G.; Cornuz, J.; Hayoz, D.; Bounameaux, H. Diagnosing Pulmonary Embolism in Outpatients with Clinical Assessment, D-dimer Measurement, Venous Ultrasound, and Helical Computed Tomography: A Multicenter Management Study. *Am. J. Med.* **2004**, *116*, 291–299.
- (7) Liu, R. S.; Chang, C. P.; Guo, W. Y.; Pan, D. H.; Ho, D. M.; Chang, C. W.; Yang, B. H.; Wu, L. C.; Yeh, S. H. ^{11}C -Acetate versus ^{18}F -FDG PET in Detection of Meningioma and Monitoring the Effect of Gamma-Knife Radiosurgery. *J. Nucl. Med.* **2010**, *51*, 883–891.
- (8) Uppal, R.; Catana, C.; Ay, I.; Benner, T.; Sorensen, A. G.; Caravan, P. Bimodal Thrombus Imaging: Simultaneous PET/MR Imaging with a Fibrin-Targeted Dual PET/MR Probe-Feasibility Study in Rat Model. *Radiology* **2011**, *258*, 812–820.
- (9) Lettau, M.; Laible, M.; Barrows, R. J.; Heiland, S.; Bendszus, M.; Hahnel, S. 3-T Contrast-Enhanced MR Angiography with Parallel Imaging in Cerebral Venous and Sinus Thrombosis. *J. Neuroradiol.* **2011**, *38*, 275–282.
- (10) Hagiwara, K.; Nishioka, T.; Suzuki, R.; Takizawa, T.; Maruyama, K.; Takase, B.; Ishihara, M.; Kurita, A.; Yoshimoto, N.; Ohsuzu, F.; Kikuchi, M. Enhancement of Ultrasonic Thrombus Imaging Using Novel Liposomal Bubbles Targeting Activated Platelet Glycoprotein IIb/IIIa Complex—*In Vitro* and *In Vivo* Study. *Int. J. Cardiol.* **2011**, *152*, 202–206.
- (11) Wang, L. V.; Gao, L. Photoacoustic Microscopy and Computed Tomography: from Bench to Bedside. *Annu. Rev. Biomed. Eng.* **2014**, *16*, 155–185.
- (12) Zhou, Y.; Yao, J.; Wang, L. V. Tutorial on Photoacoustic Tomography. *J. Biomed. Opt.* **2016**, *21*, 061007.
- (13) Xi, L.; Li, X.; Yao, L.; Grobmyer, S.; Jiang, H. Design and Evaluation of a Hybrid Photoacoustic Tomography and Diffuse Optical Tomography System for Breast Cancer Detection. *Med. Phys.* **2012**, *39*, 2584–2594.
- (14) Dogra, V. S.; Chinni, B. K.; Valluru, K. S.; Moalem, J.; Giampoli, E. J.; Evans, K.; Rao, N. A. Preliminary Results of *Ex Vivo* Multispectral Photoacoustic Imaging in the Management of Thyroid Cancer. *AJR, Am. J. Roentgenol.* **2014**, *202*, 552–558.
- (15) Karpouk, A. B.; Aglyamov, S. R.; Mallidi, S.; Shah, J.; Scott, W. G.; Rubin, J. M.; Emelianov, S. Y. Combined Ultrasound and Photoacoustic Imaging to Detect and Stage Deep Vein Thrombosis: Phantom and *Ex Vivo* Studies. *J. Biomed. Opt.* **2008**, *13*, 054061.
- (16) Song, L.; Maslov, K.; Bitton, R.; Shung, K. K.; Wang, L. V. Fast 3-D Dark-field Reflection-Mode Photoacoustic Microscopy *In Vivo* with a 30-MHz Ultrasound Linear Array. *J. Biomed. Opt.* **2008**, *13*, 054028.
- (17) Ashok, B.; Arleth, L.; Hjelm, R. P.; Rubinstein, I.; Onyuksel, H. *In Vitro* Characterization of PEG Ylated Phospholipid Micelles for Improved Drug Solubilization: Effects of PEG Chain Length and PC Incorporation. *J. Pharm. Sci.* **2004**, *93*, 2476–2487.
- (18) Pan, D.; Pramanik, M.; Senpan, A.; Yang, X.; Song, K. H.; Scott, M. J.; Zhang, H.; Gaffney, P. J.; Wickline, S. A.; Wang, L. V.; Lanza, G. M. Molecular Photoacoustic Tomography with Colloidal Nanobeacons. *Angew. Chem., Int. Ed.* **2009**, *48*, 4170–4173.
- (19) Ripoll, J.; Koberstein-Schwarz, B.; Ntziachristos, V. Unleashing Optics and Optoacoustics for Developmental Biology. *Trends Biotechnol.* **2015**, *33*, 679–691.
- (20) Song, J.; Yang, X.; Jacobson, O.; Huang, P.; Sun, X.; Lin, L.; Yan, X.; Niu, G.; Ma, Q.; Chen, X. Ultrasmall Gold Nanorod Vesicles with Enhanced Tumor Accumulation and Fast Excretion from the Body for Cancer Therapy. *Adv. Mater.* **2015**, *27*, 4910–4917.
- (21) Song, J.; Huang, P.; Duan, H.; Chen, X. Plasmonic Vesicles of Amphiphilic Nanocrystals: Optically Active Multifunctional Platform for Cancer Diagnosis and Therapy. *Acc. Chem. Res.* **2015**, *48*, 2506–2515.
- (22) Maji, S. K.; Sreejith, S.; Joseph, J.; Lin, M.; He, T.; Tong, Y.; Sun, H.; Yu, S. W.; Zhao, Y. Upconversion Nanoparticles as a Contrast Agent for Photoacoustic Imaging in Live Mice. *Adv. Mater.* **2014**, *26*, 5633–5638.
- (23) Yang, K.; Hu, L.; Ma, X.; Ye, S.; Cheng, L.; Shi, X.; Li, C.; Li, Y.; Liu, Z. Multimodal Imaging Guided Photothermal Therapy Using Functionalized Graphene Nanosheets Anchored with Magnetic Nanoparticles. *Adv. Mater.* **2012**, *24*, 1868–1872.
- (24) de la Zerda, A.; Zavaleta, C.; Keren, S.; Vaithilingam, S.; Bodapati, S.; Liu, Z.; Levi, J.; Smith, B. R.; Ma, T. J.; Oralkan, O.; Cheng, Z.; Chen, X.; Dai, H.; Khuri-Yakub, B. T.; Gambhir, S. S. Carbon Nanotubes as Photoacoustic Molecular Imaging Agents in Living Mice. *Nat. Nanotechnol.* **2008**, *3*, 557–562.
- (25) Krishna, V.; Singh, A.; Sharma, P.; Iwakuma, N.; Wang, Q.; Zhang, Q.; Knapik, J.; Jiang, H.; Grobmyer, S. R.; Koopman, B.; Moudgil, B. Polyhydroxy Fullerenes for Non-Invasive Cancer Imaging and Therapy. *Small* **2010**, *6*, 2236–2241.
- (26) Weber, J.; Beard, P. C.; Bohndiek, S. E. Contrast Agents for Molecular Photoacoustic Imaging. *Nat. Methods* **2016**, *13*, 639–650.
- (27) Shuhendler, A. J.; Pu, K.; Cui, L.; Uetrecht, J. P.; Rao, J. Real-Time Imaging of Oxidative and Nitrosative Stress in the Liver of Live Animals for Drug-toxicity Testing. *Nat. Biotechnol.* **2014**, *32*, 373–380.
- (28) Lyu, Y.; Zhen, X.; Miao, Y.; Pu, K. Reaction-Based Semiconducting Polymer Nanoprobes for Photoacoustic Imaging of Protein Sulfenic Acids. *ACS Nano* **2017**, *11*, 358–367.
- (29) Lyu, Y.; Xie, C.; Chechetka, S. A.; Miyako, E.; Pu, K. Semiconducting Polymer Nanobiocjugates for Targeted Photothermal Activation of Neurons. *J. Am. Chem. Soc.* **2016**, *138*, 9049–9052.
- (30) Lyu, Y.; Fang, Y.; Miao, Q.; Zhen, X.; Ding, D.; Pu, K. Intraparticle Molecular Orbital Engineering of Semiconducting Polymer Nanoparticles as Amplified Theranostics for *In Vivo* Photoacoustic Imaging and Photothermal Therapy. *ACS Nano* **2016**, *10*, 4472–4481.
- (31) Nie, L.; Chen, X. Structural and Functional Photoacoustic Molecular Tomography Aided by Emerging Contrast Agents. *Chem. Soc. Rev.* **2014**, *43*, 7132–7170.
- (32) de la Zerda, A.; Liu, Z.; Bodapati, S.; Teed, R.; Vaithilingam, S.; Khuri-Yakub, B. T.; Chen, X.; Dai, H.; Gambhir, S. S. Ultrahigh Sensitivity Carbon Nanotube Agents for Photoacoustic Molecular Imaging in Living Mice. *Nano Lett.* **2010**, *10*, 2168–2172.
- (33) Miao, Q.; Lyu, Y.; Ding, D.; Pu, K. Semiconducting Oligomer Nanoparticles as an Activatable Photoacoustic Probe with Amplified Brightness for *In Vivo* Imaging of pH. *Adv. Mater.* **2016**, *28*, 3662–3668.
- (34) Chen, Q.; Liu, X.; Chen, J.; Zeng, J.; Cheng, Z.; Liu, Z. A Self-Assembled Albumin-Based Nanoprobe for *In Vivo* Ratiometric Photoacoustic pH Imaging. *Adv. Mater.* **2015**, *27*, 6820–6827.
- (35) Chan, J. M.; Zhang, L.; Yuet, K. P.; Liao, G.; Rhee, J. W.; Langer, R.; Farokhzad, O. C. PLGA-Lecithin-PEG Core-Shell Nanoparticles for Controlled Drug Delivery. *Biomaterials* **2009**, *30*, 1627–1634.
- (36) Kaiser, T. E.; Stepanenko, V.; Wurthner, F. Fluorescent J-Aggregates of Core-Substituted Perylene Bisimides: Studies on Structure-Property Relationship, Nucleation-Elongation Mechanism, and Sergeants-and-Soldiers Principle. *J. Am. Chem. Soc.* **2009**, *131*, 6719–6732.
- (37) Chen, Z.; Zheng, Y.; Yan, H.; Facchetti, A. Naphthalenedi-carboximide-vs Perylenedicarboximide-Based Copolymers. Synthesis and Semiconducting Properties in Bottom-Gate N-Channel Organic Transistors. *J. Am. Chem. Soc.* **2009**, *131*, 8–9.
- (38) Fan, Q.; Cheng, K.; Yang, Z.; Zhang, R.; Yang, M.; Hu, X.; Ma, X.; Bu, L.; Lu, X.; Xiong, X.; Huang, W.; Zhao, H.; Cheng, Z. Perylene-Diimide-Based Nanoparticles as Highly Efficient Photoacoustic Agents for Deep Brain Tumor Imaging in Living Mice. *Adv. Mater.* **2015**, *27*, 843–847.
- (39) Schottler, S.; Becker, G.; Winzen, S.; Steinbach, T.; Mohr, K.; Landfester, K.; Mailander, V.; Wurm, F. R. Protein Adsorption Is Required for Stealth Effect of Poly(Ethylene Glycol)- and Poly-(Phosphoester)-Coated Nanocarriers. *Nat. Nanotechnol.* **2016**, *11*, 372–377.
- (40) Radomski, A.; Jurasz, P.; Alonso-Escolano, D.; Drews, M.; Morandi, M.; Malinski, T.; Radomski, M. W. Nanoparticle-Induced

Platelet Aggregation and Vascular Thrombosis. *Br. J. Pharmacol.* **2005**, *146*, 882–893.

(41) von zur Muhlen, C.; von Elverfeldt, D.; Moeller, J. A.; Choudhury, R. P.; Paul, D.; Hagemeyer, C. E.; Olschewski, M.; Becker, A.; Neudorfer, L.; Bassler, N.; Schwarz, M.; Bode, C.; Peter, K. Magnetic Resonance Imaging Contrast Agent Targeted Toward Activated Platelets Allows *In Vivo* Detection of Thrombosis and Monitoring of Thrombolysis. *Circulation* **2008**, *118*, 258–267.

(42) Zhou, Y.; Chakraborty, S.; Liu, S. Radiolabeled Cyclic RGD Peptides as Radiotracers for Imaging Tumors and Thrombosis by SPECT. *Theranostics* **2011**, *1*, 58–82.

(43) Schwarz, M.; Meade, G.; Stoll, P.; Ylanne, J.; Bassler, N.; Chen, Y. C.; Hagemeyer, C. E.; Ahrens, I.; Moran, N.; Kenny, D.; Fitzgerald, D.; Bode, C.; Peter, K. Conformation-Specific Blockade of the Integrin GPIIb/IIIa: A Novel Antiplatelet Strategy that Selectively Targets Activated Platelets. *Circ. Res.* **2006**, *99*, 25–33.

(44) Yan, B.; Hu, D. D.; Knowles, S. K.; Smith, J. W. Probing Chemical and Conformational Differences in the Resting and Active Conformers of Platelet Integrin Alpha(IIb)Beta(3). *J. Biol. Chem.* **2000**, *275*, 7249–7260.

(45) Iczkiewicz, J.; Broom, L.; Cooper, J. D.; Wong, A. M.; Rose, S.; Jenner, P. The RGD-Containing Peptide Fragment of Osteopontin Protects Tyrosine Hydroxylase Positive Cells Against Toxic Insult in Primary Ventral Mesencephalic Cultures and in the Rat Substantia Nigra. *J. Neurochem.* **2010**, *114*, 1792–1804.

(46) Alonso, A.; Della Martina, A.; Stroick, M.; Fatar, M.; Griebe, M.; Pochon, S.; Schneider, M.; Hennerici, M.; Allemann, E.; Meairs, S. Molecular Imaging of Human Thrombus with Novel Abciximab Immunobubbles and Ultrasound. *Stroke* **2007**, *38*, 1508–1514.

(47) Fan, Q.; Cheng, K.; Hu, X.; Ma, X.; Zhang, R.; Yang, M.; Lu, X.; Xing, L.; Huang, W.; Gambhir, S. S.; Cheng, Z. Transferring Biomarker into Molecular Probe: Melanin Nanoparticle as a Naturally Active Platform for Multimodality Imaging. *J. Am. Chem. Soc.* **2014**, *136*, 15185–15194.

(48) Hu, S. Emerging Concepts in Functional and Molecular Photoacoustic Imaging. *Curr. Opin. Chem. Biol.* **2016**, *33*, 25–31.

(49) Wang, S.; Huang, P.; Chen, X. Y. Hierarchical Targeting Strategy for Enhanced Tumor Tissue Accumulation/Retention and Cellular Internalization. *Adv. Mater.* **2016**, *28*, 7340–7364.

(50) Wang, X.; Gkanatsas, Y.; Palasubramaniam, J.; Hohmann, J. D.; Chen, Y. C.; Lim, B.; Hagemeyer, C. E.; Peter, K. Thrombus-Targeted Theranostic Microbubbles: A New Technology Towards Concurrent Rapid Ultrasound Diagnosis and Bleeding-Free Fibrinolytic Treatment of Thrombosis. *Theranostics* **2016**, *6*, 726–738.

(51) Temme, S.; Grapentin, C.; Quast, C.; Jacoby, C.; Grandoch, M.; Ding, Z.; Owenier, C.; Mayenfels, F.; Fischer, J. W.; Schubert, R.; Schrader, J.; Flogel, U. Non-invasive Imaging of Early Venous Thrombosis by ¹⁹F Magnetic Resonance Imaging with Targeted Perfluorocarbon Nanoemulsions. *Circulation* **2015**, *131*, 1405–1414.

(52) Wang, L. V.; Hu, S. Photoacoustic Tomography: *In Vivo* Imaging from Organelles to Organs. *Science* **2012**, *335*, 1458–1462.

(53) Wu, W.; Wang, Y.; Shen, S.; Wu, J.; Guo, S.; Su, L.; Hou, F.; Wang, Z.; Liao, Y.; Bin, J. *In Vivo* Ultrasound Molecular Imaging of Inflammatory Thrombosis in Arteries with Cyclic Arg-Gly-Asp-Modified Microbubbles Targeted to Glycoprotein IIb/IIIa. *Invest. Radiol.* **2013**, *48*, 803–812.

(54) Estevez, B.; Shen, B.; Du, X. Targeting Integrin and Integrin Signaling in Treating Thrombosis. *Arterioscler., Thromb., Vasc. Biol.* **2015**, *35*, 24–29.

(55) Longmire, M.; Choyke, P. L.; Kobayashi, H. Clearance Properties of Nano-Sized Particles and Molecules as Imaging Agents: Considerations and Caveats. *Nanomedicine* **2008**, *3*, 703–717.